# **OPEN ACCESS**



# Estimating the Oblateness of Dark Matter Halos Using Neutral Hydrogen Velocity Dispersion

## **Abstract**

We derive the oblateness parameter q of the dark matter halo of a sample of gas-rich, face-on disk galaxies. We have assumed that the halos are triaxial in shape but their axes in the disk plane (a and b) are equal, so that q=c/a measures the halo flattening. We have used the H I velocity dispersion, derived from the stacked H I emission lines and the disk surface density, determined from the H I flux distribution, to determine the disk potential and the halo shape at the  $R_{25}$  and  $1.5R_{25}$  radii. We have applied our model to 20 nearby galaxies, of which six are large disk galaxies with  $M(\text{stellar}) > 10^{10}$ , eight have moderate stellar masses, and six are low-surface-brightness dwarf galaxies. Our most important result is that gas-rich galaxies that have M(gas)/M(baryons) > 0.5 have oblate halos (q < 0.55), whereas stellar-dominated galaxies have a range of q values from  $0.21 \pm 0.07$  in NGC4190 to  $1.27 \pm 0.61$  in NGC5194. Our results also suggest a positive correlation between the stellar mass and the halo oblateness q, which indicates that galaxies with massive stellar disks have a higher probability of having halos that are spherical or slightly prolate, whereas low-mass galaxies have oblate halos (q < 0.55).

*Unified Astronomy Thesaurus concepts:* Galaxy dark matter halos (1880); H I line emission (690); Interstellar line emission (844); Galaxy structure (622)

## 1. Introduction

It is now well known for several decades that galaxies are embedded in massive dark matter halos, a clear indication being the nondeclining rotation curves of spiral galaxies (Rubin et al. 1980). However, the detailed properties of the halos themselves—their masses, density profiles, radii, angular momenta, or even shapes—are not well constrained. In this study we focus on halo shapes, since recent studies show that it has a strong impact on disk dynamics, such as bar evolution (Kumar et al. 2022) or disk warping (Debattista & Sellwood 1999).

Numerical studies have shown that the halo shape evolves in the process of galaxy formation, since mass infall alters halo shapes resulting in rounder and more oblate halos (Dubinski 1994). Recent cosmological simulations also suggest that galaxy halos are triaxial, with the galaxy plane favoring circular shapes i.e.,  $b/a \approx 1$  (Prada et al. 2019) and the Milky Way type galaxies have spherical or slightly oblate shapes Chua et al. (2019); twisted halos have also been detected (Emami et al. 2021). Observational studies have used various methods to constrain halo shape, such as modeling polar rings around galaxies (Khoperskov et al. 2014), flaring of H I disks (Becquaert & Combes 1997), gas or stellar kinematics of edgeon disks (Olling 1996), globular cluster systems (Posti & Helmi 2019), and stellar streams (Helmi 2020). Although the studies are few in number, it is clear that halo shapes may vary from galaxy to galaxy. The smaller, low-luminosity galaxies appear to have oblate halos (Hayashi & Chiba 2012), whereas

Original content from this work may be used under the terms of the Creative Commons Attribution 4.0 licence. Any further distribution of this work must maintain attribution to the author(s) and the title of the work, journal citation and DOI.

the larger galaxies appear to have all types of halo shapes (Banerjee & Jog 2008; Peters et al. 2017). The halo shape may also vary within a galaxy, as suggested by observations of stellar streams in our Galaxy (Bovy et al. 2016) and nearby galaxies (Khoperskov et al. 2014).

In this paper, we present a new way to determine the halo shapes of galaxies, using the HI velocity dispersion in their extended disks. This is different from previous studies that have used the gas kinematics in the inner disks to model halo shapes (O'Brien et al. 2010). Our justification for this approach is that the dark matter halo dominates the mass distribution in the outer disks of galaxies where the stellar disk mass declines. We also use face-on disk galaxies rather than edge-on galaxies, as previously done in the literature (Banerjee & Jog 2011). Our basic method is similar to Das et al. (2020), where we have shown that halo dark matter is important for supporting the vertical structure of extended H I disks. We now take this a step further by modeling the dark matter associated with the disk as part of the halo potential. In the following sections we describe the derivation of an expression for the halo oblateness parameter q, and then apply our method to estimate q for a sample galaxies.

# 2. Derivation of Halo Oblateness Factor q

We start with the equation of vertical hydrostatic equilibrium of a disk using H I as a tracer (see Das et al. 2020 for details), where  $\sigma_{zH I}$  is the H I velocity dispersion in the z direction and  $\rho_{H I}$  is the neutral hydrogen density in the disk:

$$\frac{1}{\rho_{\rm H\,I}} \frac{d \left[\sigma_{\rm zH\,I}^2 \rho_{\rm H\,I}\right]}{dz} = -\frac{d\Phi}{dz}.\tag{1}$$

The potential is composed of contributions from the stellar disk  $(\Phi_s)$ , the H I disk  $(\Phi_g)$ , and the halo  $(\Phi_h)$ . We will also use the Poisson's equation, i.e.,  $\nabla^2 \Phi = 4\pi G \rho$ , which in the flat part of disk rotation curve becomes only dependent on the vertical mass distribution.

$$\frac{d^2\Phi}{dz^2} = 4\pi G[\rho_s + \rho_g + \rho_h] \tag{2}$$

where  $\rho_s$ ,  $\rho_g$ ,  $\rho_h$  are the densities corresponding to the stars, gas, and halo. As in Das et al. (2020), we will assume the stellar and gas disks to have exponential forms in the vertical direction, i.e.,  $\rho_s = \rho_e e^{-\frac{z}{z_e}}$  and  $\rho_s = \rho_e e^{-\frac{z}{z_e}}$ , where  $\rho_e$  and  $\rho_{g0}$  are the densities at z=0, and  $z_e$ ,  $z_{g0}$  are the vertical disk scale lengths for the stellar and gas disks respectively. Let us assume that the halo potential has a logarithmic form, i.e.,

$$\Phi_h = \frac{1}{2} v_0^2 \ln(R_c^2 + R^2 + (z/q)^2)$$
 (3)

where  $v_0$  is the flat rotation velocity of the disk,  $R_c$  is the core radius of the halo, and q is the oblateness of the halo potential or q = c/a and a = b. Integrating the first two terms on the right-hand side of Equation (2) from 0 to z, and replacing the third integral with the derivative of the halo potential  $\Phi_h$ , Equation (1) becomes

$$\frac{1}{\rho_{\rm H_{1}}} \frac{d[\sigma_{\rm zH_{1}}^{2}\rho_{\rm H_{1}}]}{dz} = -4\pi G[\rho_{e}z_{e}(1 - e^{-z/z_{e}}) + \rho_{g0}z_{g0}(1 - e^{-z/z_{g0}})] - \frac{v_{0}^{2}z}{q^{2}(R_{c}^{2} + R^{2} + (z/q)^{2})}.$$
(4)

We will take  $\rho_{\rm H~I}$  from the left-hand side onto the right side and integrate throughout from 0 to infinity ( $\infty$ ). Assuming that the density falls to 0 at higher z, and that the mean H I disk vertical velocity dispersion is  $\sigma_{\rm H~I}$ , we obtain the following.

$$\sigma_{zH_{1}}^{2}\rho_{H_{1}} = 4\pi G \rho_{e} z_{e} \left[ z_{g0} - \frac{z_{e} z_{g0}}{(z_{e} + z_{g0})} \right] + 2\pi G \rho_{g0} z_{g0}^{2} + \frac{v_{0}^{2} z_{g0}^{2}}{q^{2} R^{2}}.$$
 (5)

For evaluating the last integral we have made an important assumption that

$$R^2 \gg \frac{z^2}{q^2} + R_c^2,$$
 (6)

i.e., the radius where the H I velocity dispersion is measured is much larger than the core radius of the halo  $R_c$  and the vertical height divided by the halo oblateness q. The first part of the assumption is fine, as  $R_c$  is usually  $\ll 1$  kpc in galaxies. But the second part of the assumption depends on the value of q, as we will see in the following sections. Overall, the assumption holds well as long as Equation (5) is applied to large radii in galaxies, where the stellar disk surface density is low. This is typically beyond the  $R_{25}$  radius in galaxies.

For the outer H I disks of galaxies at  $R > R_{25}$ , the stellar mass is barely detected, so that  $\rho_e \approx 0$ , and hence the first term in Equation (5) can be dropped. We then obtain the following expression for the halo q in the H I dominated, outer disks of

galaxies.

$$q^{2} = \frac{v_{0}^{2} z_{g0}^{2}}{R^{2}} \frac{1}{(\sigma_{zH_{I}}^{2} - 2\pi G \rho_{e0} z_{g0}^{2})}$$
(7)

An important implication of Equation (7) is that for q to be positive, we should have  $\sigma_{\text{zH I}}^2 \gg 2\pi G \rho_{g0} z_{g0}^2$ . But the surface density of H I is given by  $\Sigma(\text{H I}) = 2z_{g0}$   $\rho_{g0}$  and the disk dynamical mass surface density by  $\Sigma(\text{dyn}) = \frac{\sigma_{\text{zH I}}^2}{\pi G z_{g0}}$  (Das et al. 2020). So to obtain an estimate of the halo q in a galaxy from the measurement of the outer disk H I velocity, the condition  $\Sigma(\text{dyn}) > \Sigma(\text{H I})$  should be satisfied.

In the following sections we will apply Equation (7) to determine q for a sample of nearly face-on galaxies. To simplify the equation, we will use the fact that the surface density of H I is given by  $\Sigma(\text{H I}) = 2 \int_0^\infty \rho_{\text{H I}} dz = 2 \rho_{g0} z_{g0}$  (Das et al. 2020). Then Equation (7) becomes

$$q^{2} = \frac{v_{0}^{2} z_{g0}^{2}}{R^{2}} \frac{1}{(\sigma_{zHI}^{2} - \pi G z_{e0} \Sigma(HI)}.$$
 (8)

If the flat rotation velocity  $v_0$  is in units of kilometers per second, the vertical disk scale height  $z_{g0}$  and the radius in units of kiloparsecs, the vertical H I velocity dispersion in units of meters per second, the gas surface density in  $M_{\odot}$  pc<sup>-2</sup>, and the gravitational constant  $G = 6.67 \times 10^{-8}$ , we obtain

$$q = \frac{v_0 z_{g0}}{R} \times \frac{10^3}{[\sigma_{2HI}^2 - 13.97 \times 10^6 z_{g0} \Sigma(\text{H I})]^{1/2}}$$
(9)

where  $\Sigma(H I)$  includes the correction for helium in the H I gas surface density. In the following sections we will apply the above equation, following the abovementioned units to determine the halo oblateness q.

## 3. Sample Galaxies and the Data

Our model can include only quiescent disks, and hence should satisfy the criteria described in Das et al. (2020), which are that (i) the galaxies should have extended H I disks that show very little star formation and hence are in hydrostatic equilibrium; (ii) the galaxies should be close to face-on; and (iii) they should be nearby, so that several values of the azimuthally averaged H I velocity dispersion  $\sigma_{\rm zH\,I}$  over the disk can be obtained. This last point is important for obtaining a mean value of q over the disks. There were several nearly face-on galaxies that we had to exclude because they are tidally interacting and have disturbed morphologies.

The galaxies in our sample were taken from the The H<sub>I</sub> Nearby galaxy Survey (THINGS; Walter et al. 2008), which includes mainly large gas-rich galaxies and the Local Irregulars That Trace Luminosity Extremes; The H<sub>I</sub> Nearby galaxy Survey (LITTLE THINGS; Hunter et al. 2012), which includes gas-rich irregular and dwarf galaxies. We also included two galaxies NGC 4190 and UGC 8833 from the VLA ACS Nearby galaxy Survey Treasury (VLA ANGST) survey (Ott et al. 2012). Table 1 shows the sample of 20 galaxies, of which the first eight are relatively large, massive spirals (NGC 0628, NGC 3184, NGC 4736, NGC 5194, NGC 5236, and NGC 6946), and the remaining 12 are smaller spiral, dwarf or irregular galaxies.

**Table 1**Properties of the Galaxies

Galaxy	Other Name	Туре	Distance (Mpc)	Spatial Scale (pc arcsec <sup>-1</sup> )	Incl. (deg)	R <sub>25B</sub> (arcsec)	$R_d$ (arcsec)	R <sub>d</sub> (kpc)	$(\text{km s}^{-1})$	Reference for $R_d$
NGC 0628	UGC 01149	SA(s)c, H II	7.3	35.4	7.0	360.0	70.7	2.5	146.3	Ganda et al. (2009)
NGC 3184	UGC 05557	SAB(rs)cd	11.1	53.8	16.0	255.0	56.4	0.92	158.6	Tamburro et al. (2008)
NGC 4190	UGC 07232	Im pec	2.83	13.7	29.0	54.0	21.1	0.29	44.3	Lelli et al. 2016
NGC 4214	UGC 07278	IAB(s)m	2.9	14.1	44.0	330.0	62.1	0.87	76.8	Hermelo et al. (2013)
NGC 4736	UGC 07996	(R)SA(r)ab	4.7	22.8	41.0	232.9	49.8	1.1	162.2	Casasola et al. (2017)
NGC 5194	UGC 08493;	SA(s)bc pec	8.0	38.8	41.0	232.9	78.0	3.03	209.6	Casasola et al. (2017)
NGC 5236	UGCA 366	SAB(s)c	4.5	21.8	24.0	465.7	54.0	1.18	200.2	Bicay et al. 1989
NGC 6946	UGC 11597	SAB(rs)cd	5.9	28.6	33.0	497.9	68.0	5.31	182.5	Prieto et al. (2001)
Holmberg1	DDO 63	IAB(s)m	3.9	18.9	0.0	120.0	36.0	0.68	47.9	Hunter et al. (2019)
Holmberg2	DDO50	Im	3.4	16.5	41.0	396.4	89.8	1.10	69.5	Hunter et al. (2019)
M81 dwfA	PGC 23521	Irr?	3.6	17.5	23.0	37.8	14.9	0.26	32.2	Hunter et al. (2019)
F564-V3	LSBC D564-08		8.7	42.2	35.0	19.6	12.6	0.53	40.7	Hunter et al. (2012)
IC 10	UGC 192	IBm	0.7	3.4	41.0	405.0	117.8	0.40	55.8	Hunter et al. (2012)
IC 1613	UGC 00668	IB(s)m	0.7	3.4	37.9	303.5	170.9	0.58	51.5	Hunter et al. (2012)
DDO 46	UGC 3966	Im	6.1	29.6	28.6	66.0	38.5	1.14	49.4	Hunter et al. (2012)
DDO 47	UGC 3974	IB(s)m	5.2	25.2	17.0	150.0	54.4	1.37	62.9	Hunter et al. (2012)
DDO 53	UGC 04459	Im	3.6	17.5	39.5	54	41.3	0.72	37.9	Hunter et al. (2012)
DDO 75	Sextans A	IBm	1.3	6.3	33.5	142.8	34.9	0.22	39.8	Hunter et al. (2012)
DDO 187	UGC 9128	Im	2.2	10.7	39.0	54.0	16.9	0.18	27.3	Hunter et al. (2012)
UGC 8833	PGC 049452	Im	3.1	14.9	28.0	28.8	11.3	0.17	27.3	Bremnes et al. 1999

Note. The disk flat rotation velocity  $v_0$  is derived from the baryonic Tully–Fsher relation, as described in Section 2. The last column gives the reference for the disk scale length  $R_d$ .

The procedure for determining the HI velocity dispersion across the galaxy disks as a function of radius is described in Ianjamasimanana et al. (2012) and Ianjamasimanana et al. (2017), as well as in Das et al. (2020). We basically coadded the individual velocity profiles over radial bins to obtain azimuthally averaged, high signal-to-noise ratio (S/N) velocity dispersion values for each radial bin. The stacked profiles were fitted with single Gaussian functions, where the half width of the fitted Gaussian represents the velocity dispersion of the HIgas. This method gives a better estimate of the velocity dispersion compared to the moment maps. Figure 4 in the Appendix shows the radial variation of the velocity dispersion across the galaxy disks. Its value is less than 10 km s<sup>-1</sup> at the  $R_{25}$  radius, except for a few cases (NGC 5194, NGC 4190, DDO 187, and IC 10), where  $\sigma_{\rm H\,I}$  lies between 11 and 14  $km s^{-1}$ .

The stellar masses of the galaxies were derived from midinfrared (3.6  $\mu$ m) Spitzer IRAC images of the Spitzer Infrared Nearby Galaxies Survey (Kennicutt & Armus 2003). For uniformity we have used a mass to light ratio of 0.5 for all the galaxies (McGaugh & Schombert 2014), although for the dwarfs M/L = 0.4 is often more appropriate (Schombert et al. 2022). The stellar masses are shown in Table 1. The stellar surface mass densities for six of the galaxies in Table 1 are shown in Das et al. (2020), and are similar to the others in our sample. The parameters required for q determination are  $v_0$ ,  $z_{g0}$ ,  $\Sigma$ (H I), and  $\sigma_{zH I}$ . Since the galaxies are close to face-on, we used the baryonic Tully–Fisher relation (McGaugh 2012) to derive disk rotation velocities  $v_0$ , i.e.,

$$v_0 = \left[ \frac{M(*) + 1.36M(H_I) + 1.36M(H_2)}{47} \right]^{\frac{1}{4}}$$
 (10)

where M(\*) is the galaxy stellar mass, M(H I) is the H I mass, and  $M(H_2)$  is the molecular hydrogen  $(H_2)$  gas mass (Table 2). The 1.36 factor is due to the presence of helium

(Leroy et al. 2008; Asplund et al. 2009) The galaxy distances have been adopted from the H I surveys. The disk vertical scale length  $z_{g0}$  has been derived from the disk scale radius  $R_d$  using the empirical relation  $\frac{R_d}{z_{g0}} = 8.5 \pm 2.9$  (Kregel et al. 2002). Table 2 also shows the different studies from which  $R_d$  has been obtained. The H I velocity dispersion is corrected for inclination using the formula mentioned in Das et al. (2020).

## 4. Results

In our model, q has been defined assuming the hydrostatic and vertical equilibrium of an H I disk. Hence, q can be best determined only in the outer disks of galaxies, where the contribution of the star formation associated with the stellar disk is very low. So we have determined q at two radii,  $R_{25}$  and  $1.5R_{25}$ . For these radii the stellar disk contribution is extremely low and can be neglected (see Figures 3 and 4 in Das et al. 2020).

# 4.1. The Radial Variation of q in the Disk

A clear trend is that q does not vary significantly beyond the  $R_{25}$  radius (Figure 1). For the six large galaxies that have  $M(*)>10^9~M_\odot$ , q is close to constant in the outer disk region, except for NGC 3184, which shows a spike in q at large radii. However, this spike maybe due to errors in  $\sigma_{\rm H\,I}$  measurement as the H I column density decreases at the disk edge. A similar trend is present for the less-massive galaxies ( $M(*)<10^9~M_\odot$ ), where M81dfwA shows a similar spike in q at the disk edge. The dwarf galaxy IC1613 definitely has  $q\sim1$  around  $R_{25}$  and 0.5< q<1.0 beyond that. This is an exceptional case for the dwarfs. The gas-rich dwarf DDO46 is the only galaxy that shows a significant decrease in q from q=0.5 at  $R_{25}$  to 0.3 at  $2R_{25}$ , which indicates a fairly rapid change in halo shape with increasing radius.

Table 2
Stellar and Gas Masses, and the Halo Oblateness

Galaxy	$M(*)$ $(10^8 M_{\odot})$	$M({\rm H~I})$ $(10^8~M_{\odot})$	$M({ m H}_2) \ (10^8 \ M_{\odot})$	M(gas)/M(total)	q (R <sub>25</sub> )	$q = (1.5R_{25})$
NGC 0628	$1.50 \times 10^{2}$	$3.80 \times 10^{1}$	10	0.31	$0.73 \pm 0.36$	$0.74 \pm 0.39$
NGC 3184	$2.34 \times 10^{2}$	$3.07 \times 10^{1}$	$15.85 \times 10^{2}$	0.22	$1.15 \pm 0.65$	$1.91 \pm 1.20$
NGC 4190	1.19	0.46	< 0.001	0.35	$0.21 \pm 0.07$	$0.11 \pm 0.04$
NGC 4214	$1.06 \times 10^{1}$	4.08	$10^{7}$	0.35	$0.46 \pm 0.18$	$0.36 \pm 0.14$
NGC 4736	$3.15 \times 10^{2}$	4.0	$10^{8.6}$	0.03	$0.83 \pm 0.31$	$0.69 \pm 0.26$
NGC 5194	$8.38 \times 10^{2}$	$2.54 \times 10^{1}$	$10^{9.4}$	0.08	$1.27 \pm 0.61$	$0.79 \pm 0.30$
NGC 5236	$6.88 \times 10^{2}$	$1.70 \times 10^{1}$	$3.2 \times 10^{1}$	0.09	$0.44 \pm 0.16$	$0.40 \pm 0.15$
NGC 6946	$4.10 \times 10^{2}$	$4.15 \times 10^{1}$	$10^{9.6}$	0.21	$0.97 \pm 0.53$	$1.50 \pm 0.58$
Holmberg1	0.37	1.55	< 0.17	0.85	$0.20 \pm 0.07$	$0.21 \pm 0.07$
Holmberg2	2.89	5.95	< 0.40	0.74	$0.57 \pm 0.26$	$0.79 \pm 0.32$
M81 dwfA	0.16	0.25	0	0.68	$0.27 \pm 0.08$	$0.16 \pm 0.06$
F564-V3	0.73	0.41	< 0.01	0.44	$0.52 \pm 0.11$	$0.32 \pm 0.11$
IC 10	3.72	0.60	0.02	0.19	$0.21 \pm 0.07$	$0.17 \pm 0.06$
IC 1613	2.79	0.34	0.05	0.16	$0.91 \pm 0.34$	$0.67 \pm 0.25$
DDO 46	0.26	1.86	< 0.06	0.91	$0.53 \pm 0.21$	$0.39 \pm 0.15$
DDO 47	2.07	3.89		0.72	$0.41 \pm 0.14$	$0.28 \pm 0.10$
DDO 53	0.25	0.52	•••	0.74	$0.31 \pm 0.11$	$0.27 \pm 0.09$
DDO 75	0.20	0.57	< 0.02	0.84	$0.20 \pm 0.07$	$0.11 \pm 0.04$
DDO 187	0.08	0.13	< 0.004	0.69	$0.12 \pm 0.04$	$0.09 \pm 0.03$
UGC 8833	0.08	0.13	•••	0.68	$0.19 \pm 0.05$	$0.12 \pm 0.03$

## 4.2. Variation of q with Galaxy Stellar Mass

Figure 2 and Table 2 show that galaxies with more-massive stellar masses  $(M(*) > 10^9 M_{\odot})$  have q values close to  $q \sim 1$  at  $R_{25}$  and beyond (e.g., NGC 628 and NGC 6946). The exceptions are NGC 4214 and NGC 5236. Of these two galaxies, NGC 4214 is a relatively small galaxy and close to being a dwarf (Olling 1996). In fact, based on its rotation velocity, stellar mass, and absolute B-band magnitude values, NGC 4214 has been classified as a dwarf galaxy by Leroy et al. (2008). But NGC 5236 is quite massive  $(M(*) \sim 6.9 \times 10^{10} M_{\odot})$ and so its low q value is quite surprising. For the less-massive galaxies, a large fraction of which are low surface brightness (LSB) dwarfs, q is much smaller (Figure 2 and Table 2). Six of them have q = 0.2-0.3 (Holmberg1, M81dwfA, IC10, DDO75, DDO187, and UGC8833) and three of them have q = 0.4-0.5(Holmberg2, F564-V3, and DDO46). The exception is IC1613, which has a relatively large  $q \sim 1$  value at  $R_{25}$ . Thus although 14 of the 20 galaxies follow a consistent trend of larger q with increasing stellar mass, there are clearly exceptions.

Figure 2 also shows that there is a trend for less-massive galaxies to have more oblate halos compared to massive galaxies. However, there is significant error, which mainly arises from the uncertainty in disk thickness and from  $\sigma_{\rm H\,I}$  measurements. Also, the overall q decreases slightly but significantly from the  $R_{25}$  radius to the outer  $1.5R_{25}$  radius indicating that halos generally become flatter as the radius increases. We calculated the weighted correlation coefficient using the *wCorr* program in the R Statistical Software package (v4.1.2; R Core Team 2021). We found that at the  $R_{25}$  radius the Pearson weighted correlation is 0.78 and the Spearman weighted correlation is 0.79, which are both significant. At larger radii of  $1.5R_{25}$ , the values are lower, at 0.69 and 0.71 respectively.

# 4.3. Variation of q with Stellar and Gas Mass

The more-massive galaxies have lower gas mass fractions compared to the gas-rich dwarf galaxies (Table 1). To see if the

gas mass fraction has any correlation with q, we plotted the ratio of gas to baryon mass (Figure 3), where

$$M(\text{baryon}) = M(*) + 1.36M(\text{H I}) + 1.36M(\text{H}_2)$$
 (11)

so that  $M(\text{gas}) = 1.36M(\text{H I}) + 1.36M(\text{H}_2)$ . This means that the the gas-rich galaxies have M(gas)/M(baryon) > 0.5 and lie at the right-hand side, whereas the stellar-dominated disks lie toward the left side of the plot. It is interesting to note that the gas-rich galaxies (nine of them) all have oblate halos, with q < 0.6 but the stellar-dominated galaxies have a range of q values with  $q \approx 0.2$  (very oblate) to  $q \approx 1.25$  (prolate).

# 5. Implications of Our Results

Perhaps the most important result from this study is that the gas-rich galaxies all have oblate halos at  $R_{25}$  (Figure 3). There are nine gas-rich galaxies that have  $M({\rm gas})/M({\rm baryon}>0.5$  and they are all dwarf galaxies: Holmberg1, Holmberg2, M81dwfA, DDO46, DDO53, DDO75, DDO187, F564-V3, and UGC8833. The q varies between 0.11 in DDO187 to 0.55 in Holmberg2. The stellar-dominated galaxies, however, have a variety of q values ranging from q=0.21 in IC10 to q=1.25 for NGC5194 at  $R_{25}$ . This is at first surprising as one would expect that a larger stellar mass would make the disk potential more concentrated around z=0 plane, which would produce a larger gravitational force on the halo toward the disk plane. This is similar to the adiabatic contraction of halos during galaxy formation epochs (Gnedin et al. 2004), but instead we are seeing the opposite trend.

The explanation could be due to two factors. (i) A higher halo spin in the gas-dominated galaxies, which are all low-mass dwarfs. The higher halo spin is due to tidal torques experienced during galaxy formation epochs (Peebles 1969). This also results in the spreading of the stellar disk, leading to lower disk surface densities and hence lower star formation rates (Kim & Lee 2013). So Figure 3 maybe indirect evidence that gas-rich dwarfs have larger halo spins, as well as more oblate halos compared to stellar-dominated, massive galaxies. (ii) Second, a

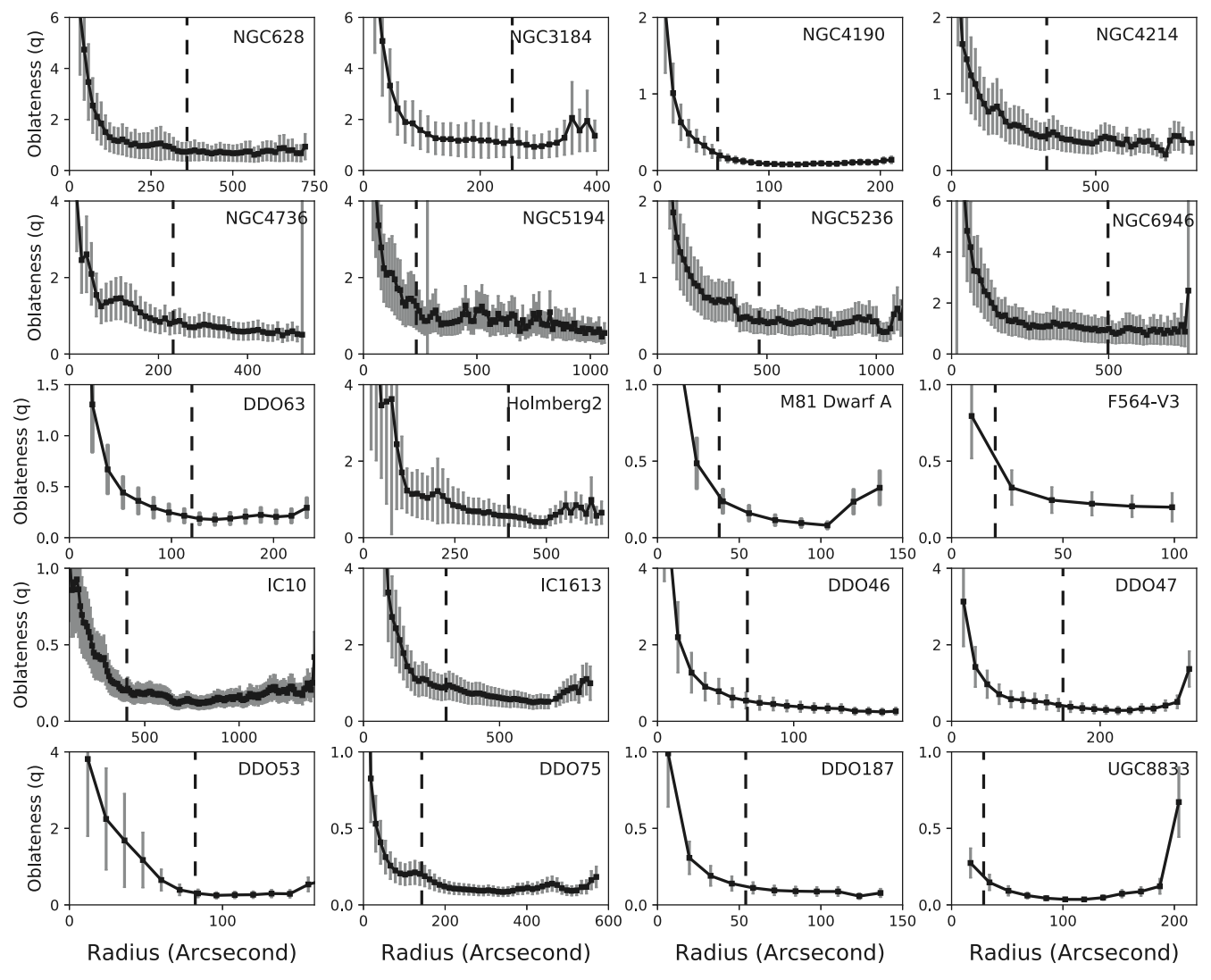
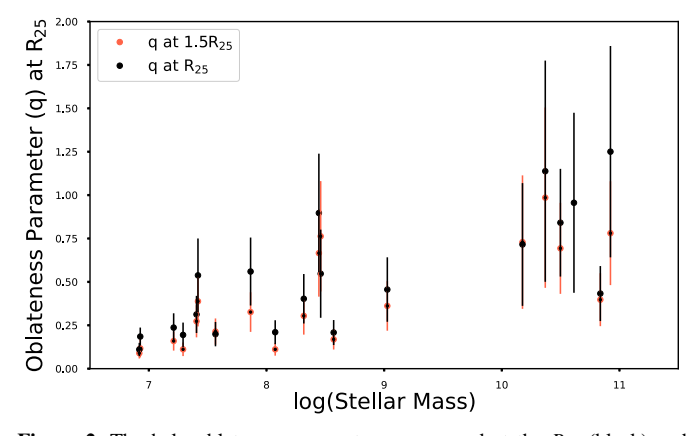
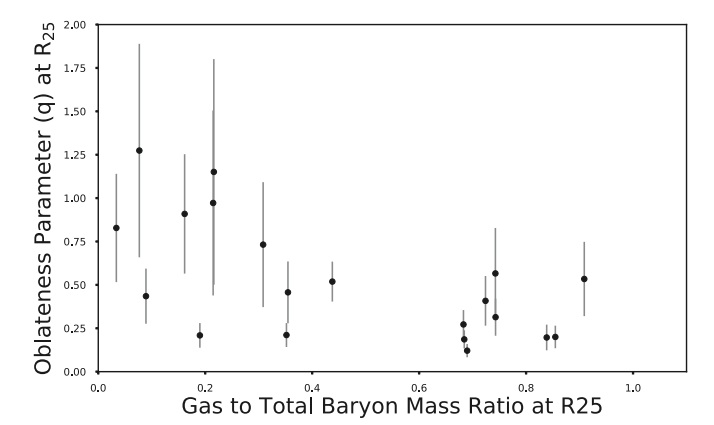


Figure 1. The halo oblateness parameter q as measured from the H I velocity dispersion plotted against the radius of the galaxy, for the large galaxies that have stellar masses  $M(*) > 10^9 M_{\odot}$ , (first two rows) and for the dwarf galaxies that have stellar masses  $M(*) < 10^9 M_{\odot}$ . The dashed line is the  $R_{25}$  radius.



**Figure 2.** The halo oblateness parameter q measured at the  $R_{25}$  (black) and  $1.5R_{25}$  radii (red) of the sample galaxies, plotted against stellar mass.

larger concentration of baryons can affect halo particle orbits, resulting in rounder halos, especially in the inner disks of galaxies (Cataldi et al. 2021). Galaxy winds and outflows associated with nuclear activity may also play an important role in making halos rounder (Chua et al. 2022) and this may ultimately affect galaxy morphology. Cosmological



**Figure 3.** Left: the halo oblateness parameter q measured at the  $R_{(25)}$  radius of a galaxy plotted against gas mass to total disk mass or baryon ratio, where the baryon mass is given as  $M(\text{baryon}) = M(*) + 1.36M(\text{H I}) + 1.36M(\text{H}_2)$ , where the 1.36 factor is the correction for the presence of helium. The gas mass is thus  $M(\text{gas}) = 1.36M(\text{H I}) + 1.36M(\text{H}_2)$ .

simulations show that galaxy mergers affect the disks of massive galaxies but affect the halo spin of only dwarf galaxies (Rodriguez-Gomez et al. 2017). These results are similar to

what we see in our study. Studies also show that halo shapes can vary with radius (Emami et al. 2021). On the observational side recent GAIA observations indicate that our Galaxy halo shape is not prolate, but instead closer spherical in shape (Hattori et al. 2021). Assuming that our Galaxy has a stellar mass of  $M(*) = 10^{11} M_{\odot}$ , Figure 4 indicates that the q for the Milky Way halo is close to q = 1 (i.e., spherical) at a radius of  $R = 1.5R_{25}$ . The errors have been derived using the propagation of errors formula. Note that the errors in q are a bit high. This is due to the large error bar in the disk height and radius  $(z - R_d)$ scaling relation. However, the intrinsic distribution of disk thicknesses is large. So it is an irreducible uncertainty because for a given face-on galaxy we do not know if it is of median thickness, or somewhat thin, or fat. It can be reduced by using a larger sample of galaxies to derive a correlation between stellar mass M(\*) and q, which will be useful for constraining cosmological models of galaxy formation and evolution.

## 6. Conclusions

We have derived the halo oblateness parameter q of a sample of 20 gas-rich, face-on disk galaxies using the H I velocity dispersion of their disks. Of these galaxies, six are large spirals with stellar masses  $>10^{10}~M_{\odot}$  and the remaining have smaller stellar masses. We find that the q remains fairly constant in the outer disk regions beyond the  $R_{25}$  radius. Our study suggests that there is a significant correlation between the stellar mass and the halo q parameter where the weighted correlation coefficient is  $\sim$ 0.78. This indicates that galaxies with massive stellar disks have a higher probability of having spherical or slightly prolate halos (0.2 < q < 1.3) whereas the low-mass dwarfs have oblate halos. On comparing q with the gas mass fractions, we find that the gas-rich galaxies with M(gas)/M

(baryons) > 0.5 all have oblate halos (q < 0.55), whereas stellar-dominated galaxies have a range of q values. Since the gas-dominated ones are all dwarfs, we conclude that gas-rich dwarf galaxies have oblate halos whereas the larger galaxies have a range q values.

M.D. acknowledges the support of the Science and Engineering Research Board (SERB) MATRICS grant MTR/ 2020/000266 for this research. R.I. acknowledges financial support from the grant CEX2021-001131-S funded by MCIN/ AEI/ 10.13039/501100011033, from the grant IAA4SKA (Ref. R18-RT-3082) from the Economic Transformation, Industry, Knowledge and Universities Council of the Regional Government of Andalusia and the European Regional Development Fund from the European Union and financial support from the grant PID2021-123930OB-C21 funded by MCIN/ AEI/10.13039/501100011033, by "ERDF A way of making Europe" and by the "European Union" and the Spanish Prototype of an SRC (SPSRC) service and support funded by the Spanish Ministry of Science and Innovation (MCIN), by the Regional Government of Andalusia and by the European Regional Development Fund (ERDF).

Facility: VLA.

*Software:* AIPS, Astropy (Astropy Collaboration et al. 2018), NumPy (Harris et al. 2020), R Statistical Software (v4.1.2; R Core Team 2021).

# Appendix The H I Velocity Dispersion Plots

The H<sub>I</sub> velocity dispersion curves that are used for calculating the galaxy halo oblateness are shown in Figure 4.

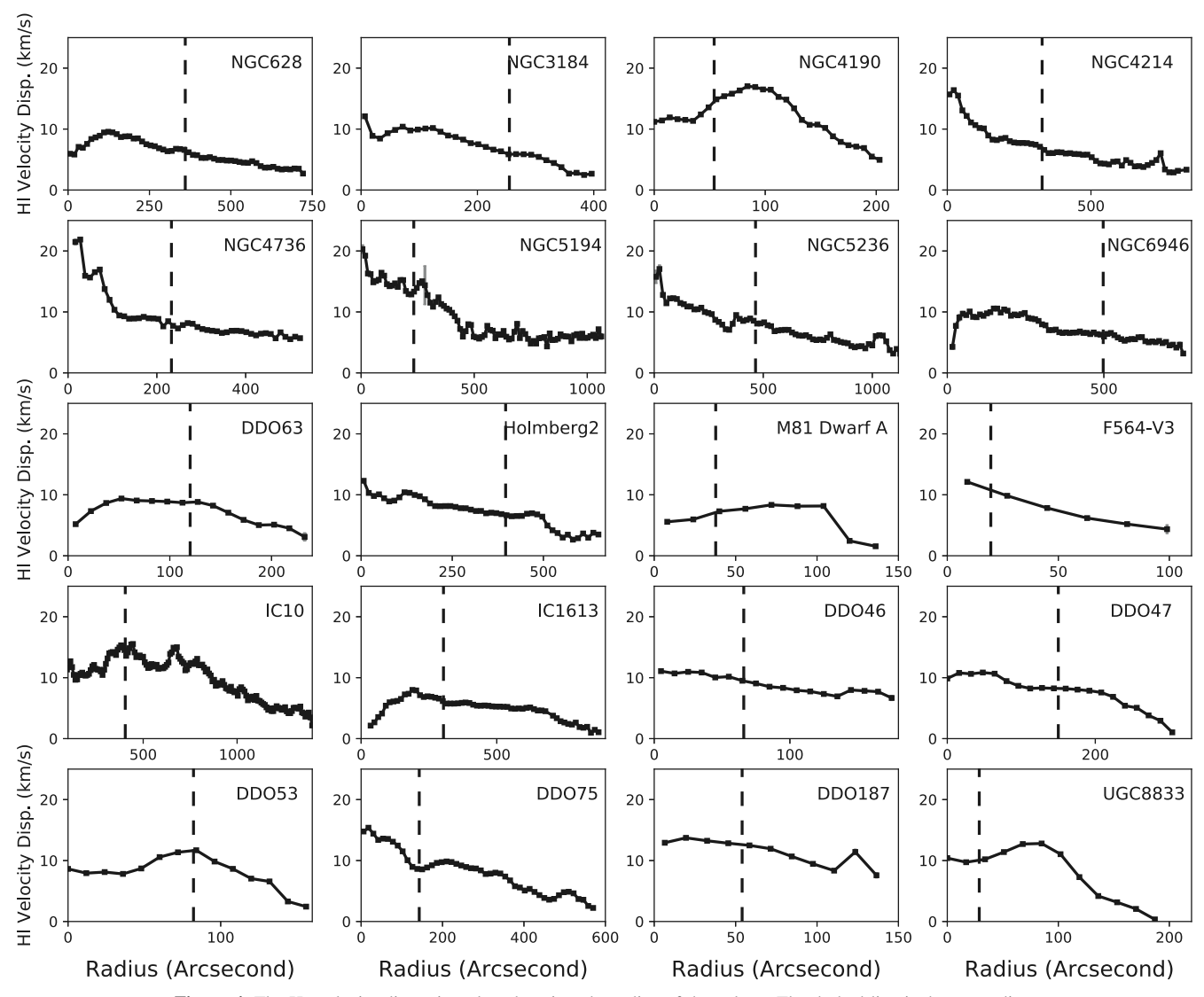


Figure 4. The H I velocity dispersion plotted against the radius of the galaxy. The dashed line is the  $R_{25}$  radius.

## **ORCID iDs**

Mousumi Das https://orcid.org/0000-0001-8996-6474 Roger Ianjamasimanana https://orcid.org/0000-0003-2476-3072

Stacy S. McGaugh https://orcid.org/0000-0002-9762-0980 James Schombert https://orcid.org/0000-0003-2022-1911

## References

Asplund, M., Grevesse, N., Sauval, A. J., & Scott, P. 2009, ARA&A, 47, 481 Astropy Collaboration, Price-Whelan, A. M., Sipőcz, B. M., et al. 2018, AJ, 156, 123

Banerjee, A., & Jog, C. J. 2008, ApJ, 685, 254 Banerjee, A., & Jog, C. J. 2011, ApJL, 732, L8 Becquaert, J. F., & Combes, F. 1997, A&A, 325, 41

Becquaert, J. F., & Combes, F. 1997, A&A, 325, 41 Bicay, M. D., Helou, G., & Condon, J. J. 1989, ApJL, 338, L53

Broy, J., Bahmanyar, A., Fritz, T. K., & Kallivayalil, N. 2016, ApJ, 833, 31 Bremnes, T., Binggeli, B., & Prugniel, P. 1999, A&AS, 137, 337 Casasola, V., Cassarà, L. P., Bianchi, S., et al. 2017, A&A, 605, A18

Cataldi, P., Pedrosa, S. E., Tissera, P. B., & Artale, M. C. 2021, MNRAS, 501, 5679

Chua, K. T. E., Pillepich, A., Vogelsberger, M., & Hernquist, L. 2019, MNRAS, 484, 476 Chua, K. T. E., Vogelsberger, M., Pillepich, A., & Hernquist, L. 2022, MNRAS, 515, 2681

Das, M., McGaugh, S. S., Ianjamasimanana, R., Schombert, J., & Dwarakanath, K. S. 2020, ApJ, 889, 10

Debattista, V. P., & Sellwood, J. A. 1999, ApJL, 513, L107

Dubinski, J. 1994, ApJ, 431, 617

Emami, R., Genel, S., Hernquist, L., et al. 2021, ApJ, 913, 36

Ganda, K., Peletier, R. F., Balcells, M., & Falcón-Barroso, J. 2009, MNRAS, 395, 1669

Gnedin, O. Y., Kravtsov, A. V., Klypin, A. A., & Nagai, D. 2004, ApJ, 616, 16 Harris, C. R., Millman, K. J., van der Walt, S. J., et al. 2020, Natur, 585, 357 Hattori, K., Valluri, M., & Vasiliev, E. 2021, MNRAS, 508, 5468

Hayashi, K., & Chiba, M. 2012, ApJ, 755, 145

Helmi, A. 2020, ARA&A, 58, 205

Hermelo, I., Lisenfeld, U., Relaño, M., et al. 2013, A&A, 549, A70

Hunter, D. A., Elmegreen, B. G., & Berger, C. L. 2019, AJ, 157, 241 Hunter, D. A., Ficut-Vicas, D., Ashley, T., et al. 2012, AJ, 144, 134

Ianjamasimanana, R., de Blok, W. J. G., & Heald, G. H. 2017, AJ, 153, 213
Ianjamasimanana, R., de Blok, W. J. G., Walter, F., & Heald, G. H. 2012, AJ, 144, 96

Kennicutt, R. C., Armus, J., Bendo, G., et al. 2003, PASP, 115, 928

Khoperskov, S. A., Moiseev, A. V., Khoperskov, A. V., & Saburova, A. S. 2014, MNRAS, 441, 2650

Kim, J.-h., & Lee, J. 2013, MNRAS, 432, 1701

Kregel, M., van der Kruit, P. C., & de Grijs, R. 2002, MNRAS, 334, 646

```
Kumar, A., Das, M., & Kataria, S. K. 2022, MNRAS, 509, 1262
Lelli, F., McGaugh, S. S., & Schombert, J. M. 2016, AJ, 152, 157
Leroy, A. K., Walter, F., Brinks, E., et al. 2008, AJ, 136, 2782
McGaugh, S. S. 2012, AJ, 143, 40
McGaugh, S. S., & Schombert, J. M. 2014, AJ, 148, 77
O'Brien, J. C., Freeman, K. C., & van der Kruit, P. C. 2010, A&A, 515, A63
Olling, R. P. 1996, AJ, 112, 481
Ott, J., Stilp, A. M., Warren, S. R., et al. 2012, AJ, 144, 123
Peebles, P. J. E. 1969, ApJ, 155, 393
Peters, S. P. C., van der Kruit, P. C., Allen, R. J., & Freeman, K. C. 2017, MNRAS, 464, 65
```

```
Posti, L., & Helmi, A. 2019, A&A, 621, A56
Prada, J., Forero-Romero, J. E., Grand, R. J. J., Pakmor, R., & Springel, V. 2019, MNRAS, 490, 4877
Prieto, M., Aguerri, J. A. L., Varela, A. M., & Muñoz-Tuñón, C. 2001, A&A, 367, 405
Rodriguez-Gomez, V., Sales, L. V., Genel, S., et al. 2017, MNRAS, 467, 3083
Rubin, V. C., Ford, W. K., & Thonnard, N, J. 1980, ApJ, 238, 471
Schombert, J., McGaugh, S., & Lelli, F. 2022, AJ, 163, 154
Tamburro, D., Rix, H. W., Walter, F., et al. 2008, AJ, 136, 2872
```

Walter, F., Brinks, E., de Blok, W. J. G., et al. 2008, AJ, 136, 2563